

# Anomalous and topological Hall effect in Cu doped $\text{Sb}_2\text{Te}_3$ topological insulator

Cite as: Appl. Phys. Lett. **117**, 092403 (2020); <https://doi.org/10.1063/5.0021722>

Submitted: 13 July 2020 . Accepted: 21 August 2020 . Published Online: 31 August 2020

Abhishek Singh, Vinod K. Gangwar, Prashant Shahi, Debarati Pal, Rahul Singh, Shiv Kumar , S. Singh, S. K. Gupta, Sudhir Kumar, Jinguang Cheng , and Sandip Chatterjee 



View Online



Export Citation



CrossMark

Lock-in Amplifiers  
up to 600 MHz



# Anomalous and topological Hall effect in Cu doped $\text{Sb}_2\text{Te}_3$ topological insulator

Cite as: Appl. Phys. Lett. **117**, 092403 (2020); doi: [10.1063/5.0021722](https://doi.org/10.1063/5.0021722)

Submitted: 13 July 2020 · Accepted: 21 August 2020 ·

Published Online: 31 August 2020



View Online



Export Citation



CrossMark

Abhishek Singh,<sup>1,a)</sup> Vinod K. Gangwar,<sup>1</sup> Prashant Shahi,<sup>2</sup> Debarati Pal,<sup>1</sup> Rahul Singh,<sup>1</sup> Shiv Kumar,<sup>3</sup> S. Singh,<sup>4</sup> S. K. Gupta,<sup>5</sup> Sudhir Kumar,<sup>6</sup> Jinguang Cheng,<sup>7</sup> and Sandip Chatterjee<sup>1,b)</sup>

## AFFILIATIONS

<sup>1</sup>Department of Physics, Indian Institute of Technology (Banaras Hindu University), Varanasi 221005, India

<sup>2</sup>Department of Physics, D.D.U. Gorakhpur University, Gorakhpur 27300, India

<sup>3</sup>Hiroshima Synchrotron Radiation Center, Hiroshima University, Higashi-Hiroshima City 739-0046, Japan

<sup>4</sup>Acoustics Instrumentation and Mechanical Systems Group, CSIR-Central Building Research Institute Roorkee, Roorkee 247667, India

<sup>5</sup>Rajshree Institute of Management and Technology, 16th km Pilibhit Road, Bareilly 243122, India

<sup>6</sup>Physics Department, Faculty of Engineering and Technology, M. J. P. Rohilkhand University, Bareilly 243006, India

<sup>7</sup>Beijing National Laboratory for Condensed Matter Physics and Institute of Physics, Chinese Academy of Sciences, Beijing 100190, China

<sup>a)</sup>Present address: Department of CMP and MS, Tata Institute of Fundamental Research, Mumbai-400005, India.

<sup>b)</sup>Author to whom correspondence should be addressed: [schatterji.app@iitbhu.ac.in](mailto:schatterji.app@iitbhu.ac.in)

## ABSTRACT

The magneto-transport and magnetization measurements of  $\text{Sb}_{1.90}\text{Cu}_{0.10}\text{Te}_3$  were performed by varying both temperature and the magnetic field. The induced antiferromagnetic ordering with Cu doping and the observed quantum oscillation in it indicate that magnetization in  $\text{Sb}_{1.90}\text{Cu}_{0.10}\text{Te}_3$  is the bulk property. The non-linearity in Hall data suggests the existence of anomalous and topological Hall effects. Moreover, the electronic band structure calculation supports the existence of Cu spin texture.

Published under license by AIP Publishing. <https://doi.org/10.1063/5.0021722>

Finding anomalous<sup>1</sup> and topological Hall effects<sup>2,3</sup> in topological materials is very promising from both basic research and application points of view. The anomalous Hall effect (AHE) exists due to the magnetic interaction of localized and conduction electrons, whereas the topological Hall effect (THE) is a hallmark of topologically non-trivial (chiral) spin textures. Generally, the THE is observed in B20 phase materials,<sup>4,5</sup> but the same has also been observed in some other kinds of materials.<sup>6–8</sup> While this phenomenon can be understood in ferromagnetic materials, recently, this has also been reported in antiferromagnetic systems.<sup>9</sup> In topologically non-trivial  $\text{HgTe}$ <sup>10,11</sup> the THE has already been predicted. However, the existence of the THE has been reported in antiferromagnetic  $\text{GdPtBi}$ ,<sup>9</sup> the electronic structure of which is similar to that of  $\text{HgTe}$ .

Moreover, recently, topological insulators (TIs) have attracted great attention of the scientific community for their interesting physical properties. The surface state in TIs, which is conducting unlike the insulating bulk state, is topologically protected by time reversal symmetry (TRS) due to the strong spin-orbit (SO) coupling.<sup>12</sup>

The delocalized topological surface states (TSSs) remain unaffected by nonmagnetic doping, and their excitation spectrum within the bulk energy gap exhibits the characteristic Dirac dispersion because of this time reversal symmetry.

On the other hand, for the spontaneously TRS broken systems, both spin-dependent scattering and the real and momentum space Berry phase<sup>12,13</sup> contribute to transverse velocity. The former is related to non-coplanar spin textures with finite scalar spin chirality, and the latter is observed in TRS-broken systems, which originates from the Berry curvature of the filled bands that is induced by the SO interaction. The magnetic texture-induced AHE is generally associated with finite spin chirality and exhibits an anomalous Hall angle of  $\sim 0.01$  (such as  $\text{SrFeO}_3$ <sup>14</sup> or  $\text{Pr}_2\text{Ir}_2\text{O}_7$ <sup>15</sup>). But in ferromagnets, the intrinsic band structure affects significantly. However, it has been suggested theoretically that non-collinear antiferromagnets may be affected by magnetic texture and strong SOC, leading to significant Hall responses.<sup>16</sup> In the present study, we have shown the existence of the THE in Cu-doped  $\text{Sb}_2\text{Te}_3$  topological insulators.

The single crystal of  $Sb_{1.90}Cu_{0.10}Te_3$  was grown by using the modified Bridgman method, as has already been reported.<sup>17</sup> The obtained crystal was easily cleaved along the (00l) direction. The chemical state of samples has been analyzed using an x-ray photoelectron spectrophotometer (XPS) (PHI Versa Probe 5000 II (ULVAC-PHI) using  $AlK\alpha$  radiation. The electrical transport properties were investigated by using a physical property measurement system (PPMS, Quantum Design). The magnetic properties were investigated by using a magnetic property measurement system (MPMS, Quantum Design).

In the present investigation, we have focused on the correlation between the magnetic structure and strong spin-orbit coupling. Magneto-transport measurements can give valuable information of the correlation of the conduction electrons to the magnetic ordering. The variation of resistivity as a function of temperature of  $Sb_{1.90}Cu_{0.10}Te_3$  has been measured. It is observed that the resistivity value increases with increasing temperature [S2].  $Sb_{1.90}Cu_{0.10}Te_3$  shows a large linear MR (nearly 45%) at low temperature, but with the increase in temperature, MR decreases (Fig. 1). For a high magnetic field, quantum oscillations were observed at low temperatures [S2]. The Landau level Fan diagram obtained from quantum oscillation shows an intercept at  $\sim -0.479$  (Fig. 1: inset), indicating that the Dirac fermions dominate the transport properties due to the additional Berry phase  $\pi$ .<sup>18</sup>

The variations of magnetization with the magnetic field as well as temperature are shown in Fig. 2. We observe that magnetization increases with the increasing magnetic field. The magnetic susceptibility ( $\chi$ ) vs T curve (inset of Fig. 2) is fitted using the following equation:

$$\chi = \chi_0 + (D \times T) + C/(T - \theta). \quad (1)$$

First, two terms in Eq. (1) describe the diamagnetic contribution in magnetic susceptibility, whereas the third term indicates the Curie-Weiss expression. The best fit of experimental data gives  $\theta = -0.46$  K, and the negative value of  $\theta$  indicates the anti-ferromagnetic nature.

For further confirmation of the anti-ferromagnetic ordering, magnetization (M) vs magnetic field (B) measurements are carried out at different temperatures. It is clear from the M vs B curve that M increases with the increase in B. Moreover, no saturation is seen even at the applied field of  $\pm 5$  T, which is a clear signature of anti-ferromagnetic

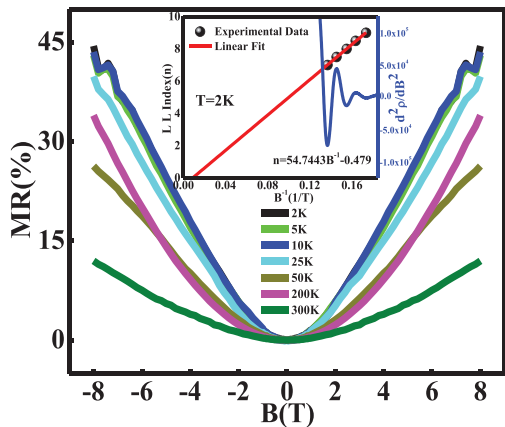


FIG. 1. (a) MR as a function of magnetic field (b) at different temperatures, Inset: SdH oscillations from the longitudinal resistance and Landau level indexing (Fan diagram) with the inverse magnetic field and linearly fitted curve (red line).

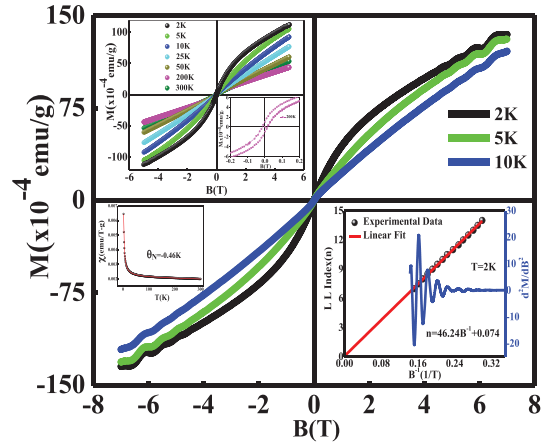


FIG. 2. Field dependence of magnetization of  $Sb_{1.90}Cu_{0.10}Te_3$  at different temperatures. Insets: temperature dependence of magnetization in ZFC mode at an applied magnetic field of 1000 Oe, magnified view of the M vs B curve at 200 K, and dHvA oscillations from the magnetization and Landau level indexing (Fan diagram) with the inverse magnetic field and linearly fitted curve (red line).

ordering. Interestingly, the nature of the curve remains anti-ferromagnetic even at room temperature (i.e., 300 K) (Fig. 2: inset). Moreover, quantum oscillation (de-Has-van-Alfen oscillation) is observed at higher fields and at low temperature ( $\leq 10$  K). The Fan level diagram (with intercept  $\sim 0.074$ ) obtained from this quantum oscillation clearly indicates the bulk contribution in the magnetic origin. Furthermore, First Fourier transform of this de-Has-van-Alfen oscillation also supports the bulk origin [S3].

Figure 3 shows the magnetic field variation of Hall resistivity at different temperatures for  $Sb_{1.90}Cu_{0.10}Te_3$ . We can easily observe three features from the  $\rho_{xy}$  vs B graph: (i) background is linear at large fields, (ii) it is non-linear at low fields, and (iii) it switches its sign from positive to negative before reaching zero field. Linearity in the graph clearly indicates the ordinary Hall effect (OHE), whereas the presence of the multicarrier and anomalous Hall effect (AHE) may be two responsible factors for the non-linearity in the Hall graph [shown in Fig. 3].

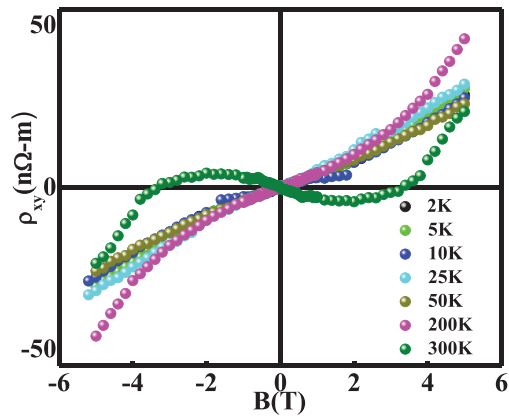


FIG. 3. Magnetic field dependence of the Hall resistivity of  $Sb_{1.90}Cu_{0.10}Te_3$  at different temperatures.

We have tried to fit the data by the two band model, but the extracted parameters were not feasible (not shown here), and therefore, multi-carrier contribution can be excluded easily. Hence, one can conclude that the AHE is the responsible factor for the nonlinearity in the graph at low fields. The presence of the AHE is also an indication of magnetic ordering.<sup>19</sup> Moreover, Hall resistivity is switching sign from positive to negative at low fields before reaching the zero value, indicating the presence of the topological Hall effect (THE).<sup>8</sup> Hence, total Hall resistivity may be expressed as the combination of three terms: OHE, AHE, and THE,

$$\rho_{xy} = R_0B + R_sM + \rho^{TH}. \tag{2}$$

Here,  $\rho_{xy}$  is the total Hall resistivity.  $R_0$  and  $R_s$  are the OHE and AHE coefficients, respectively, and  $M$  is the out-of-plane magnetization. The third term represents the topological Hall Effect. The coefficient of the anomalous Hall effect (AHE) can be represented as

$$R_s = a\rho_{xx} + b\rho_{xx}^2. \tag{3}$$

The linear and quadratic terms indicate the skew scattering and scattering independent contribution to Hall resistivity, respectively. However, consistent with the previous report, the linear term can be neglected.<sup>20,21</sup> The topological Hall effect is absent ( $\rho^{TH} = 0$ ) at high magnetic fields. It is observed that at higher fields when  $\rho^{TH} = 0$ , Eq. (2) can be simplified as

$$\frac{\rho_{xy}}{B} = R_0 + \frac{b\rho_{xx}^2M}{B}. \tag{4}$$

If we linearly fit the  $\frac{\rho_{xy}}{B}$  vs  $\frac{b\rho_{xx}^2M}{B}$  graph at the high magnetic field, we can extract  $R_0$  and  $b$  from the intercept and the slope of the curve, respectively. We obtained a very good fit at high magnetic fields with the fitting parameters  $R_0$  and  $b$  as shown in Figs. 4(a)–4(d). Subtracting ordinary Hall resistivity ( $R_0B$ ) and anomalous Hall resistivity ( $b\rho_{xx}^2M$ ) from the total Hall resistivity ( $\rho_{xy}$ ) data in the full range of magnetic fields, topological Hall resistivity ( $\rho^{TH}$ ) has been extracted. In fact, the signature of the existence of the THE is observed at very

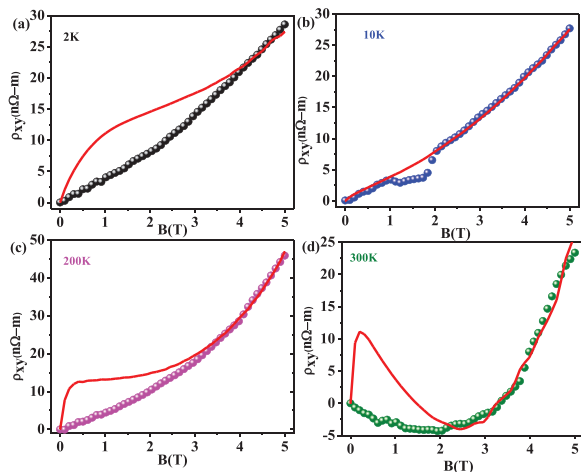


FIG. 4. (a)–(d) The fitted Hall resistivity ( $\rho_{xy}$ ) using the relation  $\rho_{xy} = R_0B + b\rho_{xx}^2M$  at temperatures 2 K, 10 K, 200 K, and 300 K, respectively.

low temperature (2 K), and at 300 K at a very low field ( $\sim 0.25$  T), it shows a maximum value (Fig. 5). Gallagher *et al.* and Yu *et al.* have shown that the THE increases with increasing temperature.<sup>5</sup> The maximum reported temperature at which the THE observed was 275 K.<sup>22</sup> But in the present investigation, the signature of the THE is found even at room temperature. Moreover, the obtained topological Hall Effect is as large as 1200 n $\Omega$  cm, which is even higher than the earlier reported values.<sup>8,23,24</sup> The highest reported value for the THE was 1800 n $\Omega$  cm, which was obtained at very low temperature, i.e., 2.5 K.<sup>9</sup> To investigate the origin of antiferromagnetism and to collect the information about the valence state and chemical bonding of the elements present in the lattice, we have used x-ray photoemission spectroscopy [S6]. It is observed from the analysis of the data that Cu is in the  $\text{Cu}^{2+}$  state, which might be a reason for the origin of antiferromagnetic ordering in the present investigation.

In fact, spin texture is the origin of the THE.<sup>25,26</sup> The linear fit of MR vs  $M^2$  [shown in Fig. 5(b)] clearly indicates the presence of spin texture in  $\text{Sb}_{1.90}\text{Cu}_{0.10}\text{Te}_3$ , which is also consistent with M(B) and M(T) analysis showing magnetic ordering. It is also clear from XPS analysis that Cu is in +2 states, i.e.,  $3d^9$  states, and hence, it should contain one unpaired electron and the corresponding magnetic moment for this state should be  $\sqrt{3}$  Bohr magneton. The spins are in anti-parallel alignment, which gives rise to the antiferromagnetic state. Moreover,

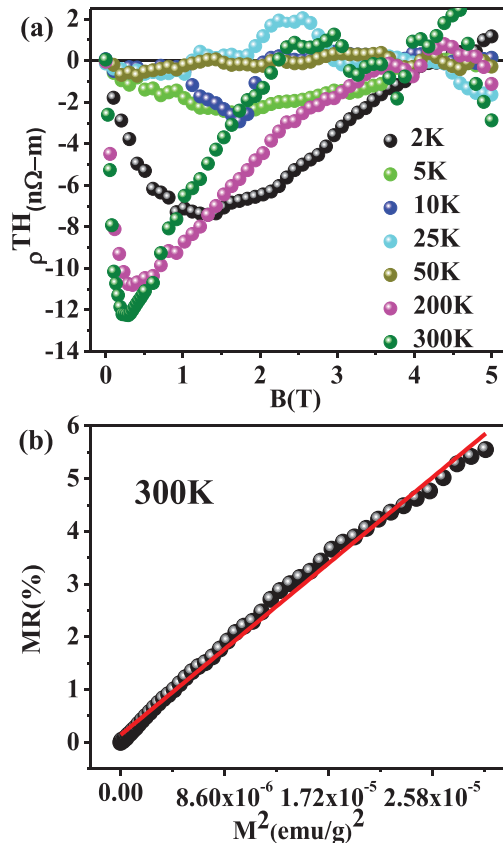


FIG. 5. (a) Topological Hall effect ( $\rho^{TH}$ ) at different temperatures as a function of magnetic field. (b) Linear fit of MR vs  $M^2$ .

from the above discussion, it is clear that even with the Cu doping, the strong spin-orbit coupling exists in this Cu-doped  $\text{Sb}_2\text{Te}_3$ . Recently, in antiferromagnets, theoretically, it is observed that a band structure-induced THE might be due to the presence of the non-collinear spin structure, which breaks both the time reversal and lattice symmetries.<sup>16,27</sup> Such a situation is observed in the present system as the cant AFM spins at a finite magnetic field. Magnetic data support both the AFM ordering and a FM canting as is evident by an increase in magnetization with the field and the existence of the hysteresis loop (Fig. 2 inset). As a matter of fact, in an AFM system with such broken time-reversal symmetry and spin-orbit coupling, the THE is predicted to be significant.

In order to unearth underlying physics of Cu-doped  $\text{Sb}_2\text{Te}_3$ , we have also carried out first principles calculations using the full potential linear Augmented Plane wave (FP-LAPW) method, which is popularly known as WIEN2K.<sup>28</sup> The exchange correlation effects are treated within local spin density approximation (LSDA) for the spin-polarized case<sup>29</sup> within the density function theory.<sup>30</sup> In the present calculations, the sphere radii of Cu, Sb, and Te are chosen to be 2.25, 2.28, and 2.28 a.u., respectively. Within these spheres, the charge density and potential are expanded in terms of crystal harmonics. The values of  $K_{\text{max}} \times R_{\text{MT}} = 7.0$  (where  $R_{\text{MT}}$  and  $K_{\text{max}}$  are the atomic sphere radii and interstitial plane wave cut-off),  $G_{\text{max}} = 14$ , and  $l_{\text{max}} = 10$  are used for charge density Fourier expansion and wave function expansions inside the sphere. We use 181 k-points in the irreducible BZ to calculate electronic and magnetic properties of Cu-doped  $\text{Sb}_2\text{Te}_3$ . We have considered the measured value of the lattice constants ( $a = 4.25 \text{ \AA}$  and  $c = 30.4 \text{ \AA}$ ) for all sets of calculations, and the atomic positions are relaxed. However, the optimized value between any two quintuple layers (QLs) equal to  $2.76 \text{ \AA}$  has been used throughout the calculation. Some general features of the relaxation are noted that the Cu atom replaces Sb that lies between two Te atoms. While with relaxation of the atomic positions, the neighboring atoms move to accommodate the smaller radius of the Te atoms, the rest of the atoms show small changes in order to maintain the original crystal structure.

We have performed detailed calculations for all the three magnetic phases of Cu-doped  $\text{Sb}_2\text{Te}_3$ , i.e., paramagnetic (PM), ferromagnetic (FM), and antiferromagnetic (AFM) phases. The calculated total energies/atom with spin-orbit coupling (SOC) for PM, FM, and AFM states are  $-12699.372906$ ,  $-12699.379561$ , and  $-12699.381522 \text{ Ry/atom}$ , respectively. The minimum value of total energy/atom suggests that the AFM phase is the most stable state. The FM state shows a very feeble magnetic moment of  $2 \times 10^{-5}$  ( $3.2467 \times 10^{-1}$ )  $\mu_B$  without (with) SOC [S7]. Further, in order to confirm the stable AFM state, we have performed detailed electronic structure calculations. The relaxed unit cell of  $\text{Sb}_5\text{CuTe}_9$  is shown in Fig. 6(a). This is important to mention that while performing the calculation for the AFM state, we took a supercell of 30 atoms. Nevertheless, the concentration of Cu in  $\text{Sb}_5\text{CuTe}_9$  is much higher than experimental realization, and therefore, calculations are performed at this concentration to understand the Cu-d states and stability of different phases. The theoretical calculation supports our experimental observation.

The calculated band structure of  $\text{Sb}_5\text{CuTe}_9$  with SOC for the AFM phase and the corresponding first Brillouin Zone (BZ) are presented in Fig. 6. The band structure shows a very narrow bandgap at the center of the BZ (Gamma), and the Fermi level lies  $\sim 140 \text{ meV}$  below the center of the gap and supports the p-type nature of the

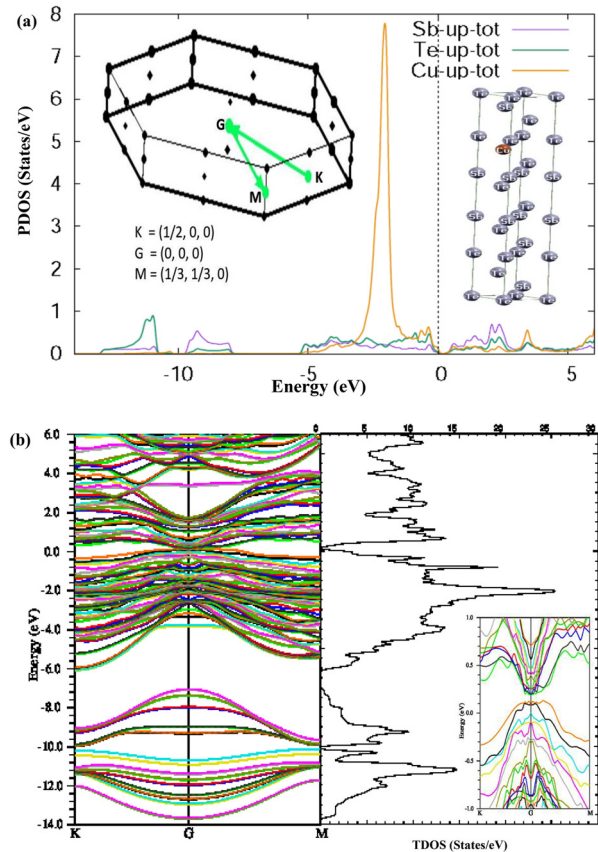


**FIG. 6.** (a) Calculated projected density of states (PDOS) for Cu, Sb, and Te. Right inset: the Crystal structure of  $\text{Sb}_5\text{CuTe}_9$ . The five atoms “quintuple layer leaves” are separated by a van der Waals gap equal to  $2.76 \text{ \AA}$ . Different colors of the spheres are marked with the corresponding element symbol. Left inset: first BZ of  $\text{Sb}_5\text{CuTe}_9$  and along the selected path corresponding to the dispersion curve. (b) Calculated band structure along M, G, and K directions for  $\text{Sb}_5\text{CuTe}_9$ , calculated total density of states (TDOS) for  $\text{Sb}_5\text{CuTe}_9$ . Inset: magnified view at the Gamma point.

sample [inset of Fig. 6(b)]. Further, in order to see the energy bandgap in-between valence band maxima (VBM) and conduction band minima (CBM), we have magnified the band structure in the energy range between  $-1.0$  and  $1.0 \text{ eV}$  as presented in the right inset of Fig. 6(b). The CBM is mainly composed of Sb-p and Cu-d with a small contribution from Te-p. The total density of states presented along with band structure shows a strong peak near  $\sim -2.1 \text{ eV}$  corresponding to Cu-d states. On the other hand, the VBM is composed of mainly the Cu-d orbital with the strong hybridization from the Te-p orbital. The layered structure of  $\text{Sb}_5\text{CuTe}_9$ , and the size mismatch between Cu and Sb/Te sites weaken the hybridization fairly by replacing Sb by Cu. The total density of states (TDOS) of  $\text{Sb}_5\text{CuTe}_9$  is presented in Fig. 6(b). The calculated TDOS shows a strong peak just below the VBM ( $\sim -2.1 \text{ eV}$ ), appearing mainly from Cu-d. At the VBM, there is strong hybridization between Cu-d and Te-p states ( $\sim -0.65 \text{ eV}$ ). On the other hand, Sb-p states are dominated in the CBM with a considerable contribution from Te-p. Moreover, the Cu-d state shows strong hybridization with Sb-p and Te-p at  $\sim 2.6 \text{ eV}$ . Overall, near the VBM,

Cu-d is dominant, while the CBM is dominated by Sb-p and Te-p shows strong hybridization between them.

However, we have discussed above spin texture as the origin of the THE in Cu-doped  $\text{Sb}_2\text{Te}_3$  at a finite magnetic field as is observed in the FM system,<sup>7,8,26</sup> if driven to anti-crossings near the Fermi level. It is also clear from Fig. 6(b) that with Cu doping, anti-crossing at the Fermi level is observed. This may carry the significant Berry curvature. The large spin-orbit coupling along with the critical band alignment may enhance the effect of the Cu spin texture on these bands. Therefore, the significant Berry phase contributes to the THE due to the development of spin texture with the evolution of the electronic structure.

In conclusion, Hall data indicate the existence of anomalous and topological Hall effects even at room temperature. Magnetization data indicate that Cu-doped  $\text{Sb}_2\text{Te}_3$  is in the AFM state. But with the application of the magnetic field, the spin structure cants ferromagnetically, which is observed from the appearance of the hysteresis loop in the M(B) curve. The observed THE might be due to the spin textures, which is clear from the linear variation of MR with  $M^2$ . The band structure confirms the existence of spin texture. We have measured the magneto-transport and magnetization at different temperatures and different fields. We find the coexistence of both bulk and surface states from the quantum oscillations. The observed room temperature antiferromagnetism is due to the  $\text{Cu}^{2+}$  spin state. Moreover, the THE has been established at room temperature, which may be very promising for spintronic devices working at room temperature.

See the [supplementary material](#) for XRD, SdH, dHvA, and XPS analysis of the  $\text{Sb}_{1.90}\text{Cu}_{0.10}\text{Te}_3$  topological insulator.

#### AUTHORS' CONTRIBUTIONS

A.S. and V.K.G. equally contributed to this work.

The authors are grateful to the CIF, IIT (BHU), for providing facility for magnetic measurements.

#### DATA AVAILABILITY

The data that support the findings of this study are available within this article and its [supplementary material](#).

#### REFERENCES

- <sup>1</sup>N. Nagaosa, J. Sinova, S. Onoda, A. H. Macdonald, and N. P. Ong, *Rev. Mod. Phys.* **82**, 1539 (2010).
- <sup>2</sup>P. Bruno, V. K. Dugaev, and M. Taillefumier, *Phys. Rev. Lett.* **93**, 096806 (2004).
- <sup>3</sup>N. Nagaosa and Y. Tokura, *Nat. Nanotechnol.* **8**, 899 (2013).
- <sup>4</sup>S. Muhlbauer, B. Binz, F. Jonietz, C. Pfleiderer, A. Rosch, A. Neubauer, R. Georgii, and P. Boni, *Science* **323**, 915 (2009).
- <sup>5</sup>X. Z. Yu, N. Kanazawa, Y. Onose, K. Kimoto, W. Z. Zhang, S. Ishiwata, Y. Matsui, and Y. Tokura, *Nat. Mater.* **10**, 106 (2011).
- <sup>6</sup>O. Boule, J. Vogel, H. Yang, S. Pizzini, D. D. S. Chaves, A. Locatelli, T. O. Menteş, A. Sala, L. D. Buda-Prejbeanu, O. Klein, M. Belméguenai, Y. Roussigné, A. Stashkevich, S. M. Chérif, L. Aballe, M. Foerster, M. Chshiev, S. Auffret, I. M. Miron, and G. Gaudin, *Nat. Nanotechnol.* **11**, 449 (2016).
- <sup>7</sup>S. X. Huang and C. L. Chien, *Phys. Rev. Lett.* **108**, 267201 (2012).
- <sup>8</sup>Y. Li, N. Kanazawa, X. Z. Yu, A. T. Sukazaki, M. Kawasaki, M. Ichikawa, X. F. Jin, F. Kagawa, and Y. Tokura, *Phys. Rev. Lett.* **110**, 117202 (2013).
- <sup>9</sup>T. Suzuki, R. Chisnell, A. Devarakonda, Y.-T. Liu, W. Feng, D. Xiao, J. W. Lynn, and J. G. Checkelsky, *Nat. Phys.* **12**, 1119 (2016).
- <sup>10</sup>B. A. Bernevig, T. L. Hughes, and S.-C. Zhang, *Science* **314**, 1757 (2006).
- <sup>11</sup>M. König, S. Wiedmann, C. Brune, A. Roth, H. Buhmann, L. W. Molenkamp, X.-L. Qi, and S.-C. Zhang, *Science* **318**, 766 (2007).
- <sup>12</sup>M. Z. Hasan and C. L. Kane, *Rev. Mod. Phys.* **82**, 3045 (2010).
- <sup>13</sup>J. Ye, Y. B. Kim, A. J. Millis, B. I. Shraiman, P. Majumdar, and Z. Tešanović, *Phys. Rev. Lett.* **83**, 3737 (1999).
- <sup>14</sup>S. Ishiwata, M. Tokunaga, Y. Kaneko, D. Okuyama, Y. Tokunaga, S. Wakimoto, K. Kakurai, T. Arima, Y. Taguchi, and Y. Tokura, *Phys. Rev. B* **84**, 054427 (2011).
- <sup>15</sup>Y. Machida, S. Nakatsuji, Y. Maeno, T. Tayama, T. Sakakibara, and S. Onoda, *Phys. Rev. Lett.* **98**, 057203 (2007).
- <sup>16</sup>C. Sürgers, G. Fischer, P. Winkel, and H. V. Löhneysen, *Nat. Commun.* **5**, 3400 (2014).
- <sup>17</sup>A. Singh, A. K. Ghosh, and S. Chatterjee, *J. Supercond. Novel Magn.* **31**, 299 (2018).
- <sup>18</sup>R. Singh, V. K. Gangwar, D. D. Daga, A. Singh, A. K. Ghosh, M. Kumar, A. Lakhani, R. Singh, and S. Chatterjee, *Appl. Phys. Lett.* **112**, 102401 (2018).
- <sup>19</sup>H. Chen, Q. Niu, and A. H. Macdonald, *Phys. Rev. Lett.* **112**, 017205 (2014).
- <sup>20</sup>Y. Tian, L. Ye, and X. Jin, *Phys. Rev. Lett.* **103**, 087206 (2009).
- <sup>21</sup>N. A. Porter, J. C. Gartside, and C. H. Marrows, *Phys. Rev. B* **90**, 024403 (2014).
- <sup>22</sup>J. C. Gallagher, K. Y. Meng, J. T. Brangham, H. L. Wang, B. D. Esser, D. W. McComb, and F. Y. Yang, *Phys. Rev. Lett.* **118**, 027201 (2017).
- <sup>23</sup>Y. Ohuchi, Y. Kozuka, M. Uchida, K. Ueno, A. Tsukazaki, and M. Kawasaki, *Phys. Rev. B* **91**, 245115 (2015).
- <sup>24</sup>N. Kanazawa, Y. Onose, T. Arima, D. Okuyama, K. Ohoyama, S. Wakimoto, K. Kakurai, S. Ishiwata, and Y. Tokura, *Phys. Rev. Lett.* **106**, 156603 (2011).
- <sup>25</sup>I. Dzyaloshinsky, *J. Phys. Chem. Solids* **4**, 241 (1958).
- <sup>26</sup>T. Moriya, *Phys. Rev.* **120**, 91 (1960).
- <sup>27</sup>S. Nakatsuji, N. Kiyohara, and T. Higo, *Nature* **527**, 212 (2015).
- <sup>28</sup>P. Blaha, K. Schwarz, P. Sorantin, and S. Trickey, *Comput. Phys. Commun.* **59**, 399 (1990).
- <sup>29</sup>U. V. Barth and L. Hedin, *J. Phys. C* **5**, 1629 (1972).
- <sup>30</sup>W. Kohn and L. J. Sham, *Phys. Rev. A* **140**, A1133 (1965).